Chem

CellPress

Article

Hydrogen atom abstraction by a high-spin [Fe^{III}=S] complex

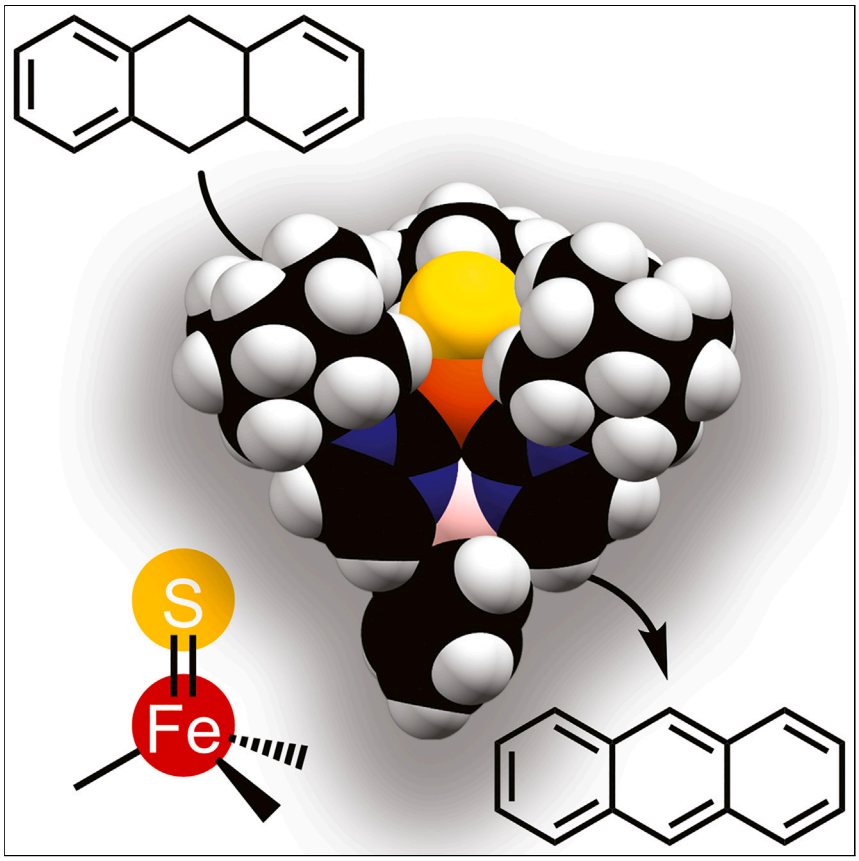

Due to their intrinsic reactivity, there is still limited understanding of the fundamental properties and reactivity of late metal sulfides $[M=S]^{n+}$. Here, we show that an appropriate supporting ligand allows the elementary unit of ubiquitous iron-sulfur clusters, namely, the $[Fe=S]^{n+}$ fragment, to be isolated and structurally characterized for the first time. Experimental insights also provide a point of comparison with the analogous iron oxo unit, a common intermediate in enzymatic oxidations.

Juan A. Valdez-Moreira, Duleeka C. Wannipurage, Maren Pink, Veronica Carta, Pierre Moënne-Loccoz, Joshua Telser, Jeremy M. Smith

smith962@indiana.edu

Highlights

Synthesis and characterization of a terminal iron sulfide complex

Structural, spectroscopic, and computational support for Fe=S character

Dihydroanthracene oxidation reactivity analogous to terminal iron oxide complexes

Valdez-Moreira et al., Chem 9, 1–9
September 14, 2023
https://doi.org/10.1016/j.chempr.2023.05.007

Please cite this article in press as: Valdez-Moreira et al., Hydrogen atom abstraction by a high-spin [Fe^{III}=S] complex, Chem (2023), https://doi.org/10.1016/j.chempr.2023.05.007

Chem

CellPress

Article

Hydrogen atom abstraction by a high-spin [Fe^{III}=S] complex

Juan A. Valdez-Moreira,[1,4] Duleeka C. Wannipurage,[1,4] Maren Pink,[1] Veronica Carta,[1] Pierre Moënne-Loccoz,[2] Joshua Telser,[3] and Jeremy M. Smith[1,5,*]

SUMMARY

Iron-sulfur clusters are critical to a plethora of biological processes; however, little is known about the elementary unit of these clusters, namely, the $[Fe=S]^{n+}$ fragment. Here, we report the synthesis and characterization of a terminal iron sulfido complex. Despite its high-spin (S = 5/2) ground state, structural, spectroscopic, and computational characterization provide evidence for iron sulfur multiple bond character. Intriguingly, the complex reacts with additional sulfur to afford an S = 3/2 iron(III) disulfido (S_2^{2-}) complex. Preliminary studies reveal that the sulfido complex reacts with dihydroanthracene to afford an iron(II) hydrosulfido complex, akin to the reactivity of iron oxo complexes. By contrast, there is no reaction with the disulfido complex. These results provide important insight into the nature of the iron sulfide unit.

INTRODUCTION

Although best known for their role in electron transfer, iron-sulfur clusters are critical to many biological processes, including cellular respiration, enzyme catalysis, sulfur donation, sensing, and gene expression.[1–3] In addition to the common [2Fe-2S], [3Fe-4S], and [4Fe-4S] clusters, more complex iron-sulfur clusters are also known, such as the [8Fe-7S] double cubane P cluster of nitrogenase.[4,5] By creating well-defined model complexes, synthetic chemistry has played an important role in delineating the properties of these clusters.[3,6,7] Among these model complexes are smaller iron-sulfur clusters that provide essential elements of their higher nuclearity brethren, e.g., low-coordinate [2Fe-1S] clusters model the Fe–S–Fe belt units of the larger Fe_7MoS_9C cluster (FeMoco) that is the active site of nitrogenase.[8–14]

The elementary unit of all iron-sulfur clusters is the iron-inorganic sulfide fragment, i.e., $[Fe=S]^{n+}$—the [1Fe-1S] "cluster"; however, there is limited knowledge of its properties. This is principally due to the lack of terminal iron sulfido complexes that would serve as appropriate models for the $[Fe=S]^{n+}$ unit. Although computational studies of hypothetical iron(IV) sulfido species suggest an oxidizing power similar to that of the better studied iron(IV) oxo complexes, experimental verification is lacking.[15,16] Indeed, only one example of an iron sulfido complex is known, which is notable for a stabilizing second coordination sphere hydrogen bond network that attenuates the iron-sulfur multiple bond character and hence its reactivity.[17,18] The paucity of iron sulfido complexes reflects the rarity of late metal sulfido complexes in general.[19] Apart from unobserved transient species that have been proposed as reaction intermediates,[20–26] to date, all examples of late metal sulfido complexes are protected by alkali metal ion capping groups.[27–29]

THE BIGGER PICTURE

Late metal sulfides $[M=S]^{n+}$ are proposed as intermediates in the activity of several metalloenzymes and industrial catalysts. Although well-defined model compounds might be expected to provide insight into these fleeting species, the intrinsic reactivity of this unit has hindered efforts to access complexes containing this entity. Consequently, there is still limited understanding of the fundamental properties and reactivity of the $[M=S]^{n+}$ fragment. Here, we show that an appropriate supporting ligand allows the elementary unit of ubiquitous iron-sulfur clusters, namely, the $[Fe=S]^{n+}$ fragment, to be isolated for the first time. Experimental insights into the structure and properties of this terminal iron sulfido complex also provide a point of comparison with the analogous iron oxo unit, a common intermediate in enzymatic oxidations.

Please cite this article in press as: Valdez-Moreira et al., Hydrogen atom abstraction by a high-spin [Fe^{III}=S] complex, Chem (2023), https://doi.org/10.1016/j.chempr.2023.05.007

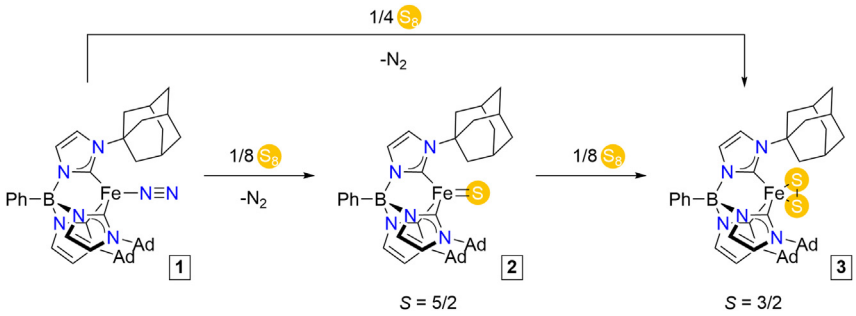

Scheme 1. Synthesis of iron sulfido and disulfido complexes

Building on our extensive investigations of terminal iron nitride complexes, which are based on strongly donating tris(carbene)borate ligands,[30–36] we recently reported the synthesis and characterization of a low-spin (S = 1/2) iron(III) oxo complex.[37] The absence of stabilizing second-coordination sphere interactions makes this complex distinct from other iron(III) oxo species,[38–41] leading to greater iron-oxygen multiple bond character and enhanced reactivity. Here, we report that the same bulky tris(carbene)borate ligand stabilizes an iron(III) sulfido complex that is similarly free of second-coordination sphere hydrogen bond donors. In contrast to its oxo congener, the sulfido complex adopts a high-spin (S = 5/2) ground state. Nonetheless, structural, spectroscopic, and computational investigations provide evidence for iron-sulfur multiple bond character. Preliminary reactivity studies reveal that the complex mimics at least one pathway of the corresponding iron oxo, reacting with dihydroanthracene to afford the corresponding iron(II) hydrosulfido complex.

RESULTS AND DISCUSSION

The iron(I) dinitrogen complex PhB(AdIm)$_3$Fe–N$_2$ (**1**)[42] reacts with 1/8 equiv S$_8$ to afford the dark brown iron(III) sulfido complex PhB(AdIm)$_3$Fe=S (**2**) in 84 % isolated yield (Scheme 1; Figures S1, S8, and S11). Samples of **2** are always contaminated with small quantities of a second product, identified as the disulfido complex **3**, which is discussed in more detail below.

Complex **2** has been characterized by single-crystal X-ray diffraction (Figures 1A and S31; Table S8), which reveals a trigonally symmetric complex with the Fe–S bond on the molecular 3-fold axis (B–Fe–S angle = 176.85(7)°). The coordination sphere of the iron atom is completed by the three carbene donors (Fe–C 2.088(3)–2.139(3) Å). These distances are significantly longer than for the analogous iron(III) oxo complex, which is likely a consequence of the difference in spin state (see below). These longer distances mean that the iron atom is further out the plane defined by the three carbon donor atoms than in the case of the oxo complex (≈1.2 vs. 1.1 Å).

The Fe–S bond distance in **2** (2.1173(9) Å) is slightly shorter than that observed in [Fe^{III}H$_3$buea(S)]$^{2-}$ (2.211(1) Å), which is the only other structurally characterized iron(III) sulfido complex.[17,18] However, in contrast to the latter complex, there is no evidence of stabilizing second coordination sphere hydrogen bonding interactions in **2**, with the shortest S···H contact greater than 2.9 Å. Complex **2** has good stability in low temperature (e.g., −35°C) solution, although decomposition to unknown products is observed over 24 h at 30°C. The stability of **2** likely stems from the protective effect of the tris(carbene)borate ligand, with its large adamantyl groups enveloping the sulfido ligand, as illustrated by a space-filling diagram (Figure 1B).

[1]Department of Chemistry, Indiana University, Bloomington, IN 47405, USA

[2]Department of Chemical Physiology and Biochemistry, School of Medicine, Oregon Health & Science University, Portland, OR 97239, USA

[3]Department of Biological, Physical and Health Sciences, Roosevelt University, Chicago, IL 60605, USA

[4]These authors contributed equally

[5]Lead contact

*Correspondence: smith962@indiana.edu

https://doi.org/10.1016/j.chempr.2023.05.007

Please cite this article in press as: Valdez-Moreira et al., Hydrogen atom abstraction by a high-spin [Fe^{III}=S] complex, Chem (2023), https://doi.org/10.1016/j.chempr.2023.05.007

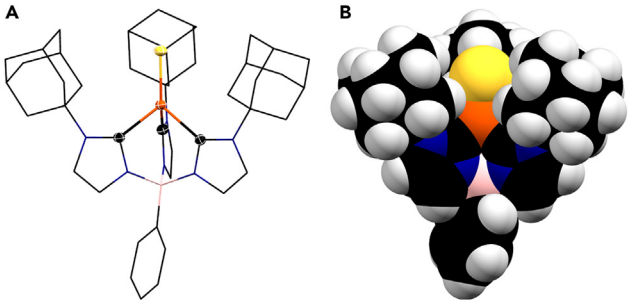

Figure 1. Structural characterization of sulfido complex 2

(A) X-ray crystal structure of $PhB(AdIm)_3Fe{=}S$, thermal ellipsoids shown at 50 % probability, hydrogen atoms omitted and most atoms of the tris(carbene)borate shown as wireframe for clarity. A 5 % component that is attributed to $PhB(AdIm)_3Fe(\kappa^2{-}S_2)$ (**3**) is also not shown.

(B) Space-filling model for the structure of **2**.

The sulfido ligand is further characterized by resonance Raman spectroscopy. Room temperature resonance Raman spectra of **2** obtained with a 407 nm excitation (Figures S11 and S13) show a very strong band at 470 cm^{-1} that downshifts 8 cm^{-1} with ^{34}S-labeling (Figure 2A), as expected from the calculated 9 cm^{-1} downshift for a harmonic Fe–S oscillator from Hooke's law. This Fe–S stretching frequency is ~100 cm^{-1} higher than in $[Fe^{III}H_3buea(S)]^{2-}$, which, using Badger's rule,[43] computes to a 0.17 Å decrease in FeS bond length in the absence of hydrogen bond partners to the sulfido ligand.

Other spectroscopic methods provide insight into the electronic structure of the iron center in **2**. An asymmetric doublet (δ = 0.24 mm s^{-1}, $|\Delta E_Q|$ = 2.38 mm s^{-1}) is observed in the solid-state ^{57}Fe Mössbauer spectrum at 80 K (Figures 2B, S14, and S15). The quadrupole doublet is more symmetric at 150 K, with significantly sharper lines, suggesting that the asymmetry arises from slow paramagnetic relaxation. It is notable that the isomer shift for **2** is distinct from that observed for the structurally related tris(carbene)borate iron(III) imido (δ = −0.11 mm/s) and iron(III) oxo (δ = −0.15 mm/s) complexes, all of which adopt a low-spin (S = 1/2) state. Indeed, the observed isomer shift is in the range observed for high-spin iron(III) complexes, suggesting a high-spin (S = 5/2) iron(III) center for complex **2**. This is supported by the results of electronic structure calculations, see below.

The high-spin-state assignment is supported by electron paramagnetic resonance (EPR) spectroscopy. An axial EPR spectrum is observed in frozen toluene (12 K), with an effective $\boldsymbol{g}'$-tensor ($\boldsymbol{g}'$ = [6.50, 5.50, 2.00]) that is most consistent with an S = 5/2 spin state (Figures 2C and S17–S19). These observed (effective S' = 1/2) g values can be related to the spin Hamiltonian parameters for the real spin system, i.e., S = 5/2.[44,45] Complex **2** is thus nearly axial, g_x = 1.99, g_y = 2.01, g_z = 2.01, E/D = 0.0195 (D > 0 and is much larger than the microwave quantum energy at X-band: ~0.31 cm^{-1}). The high-spin state is maintained in room temperature solution, as evidenced by the magnetic moment (μ_{eff} = 5.8 μ_B at 298 K).

DFT calculations (B3LYP/def2-TZVP) reproduce the observed sextet (S = 5/2) ground spin state, with the doublet (S = 1/2) and quartet (S = 3/2) states higher in energy (Tables S2 and S3). In addition, the computed ^{57}Fe Mössbauer spectral parameters for the sextet state are in reasonable agreement with the experimental values

Please cite this article in press as: Valdez-Moreira et al., Hydrogen atom abstraction by a high-spin [Fe^{III}=S] complex, Chem (2023), https://doi.org/10.1016/j.chempr.2023.05.007

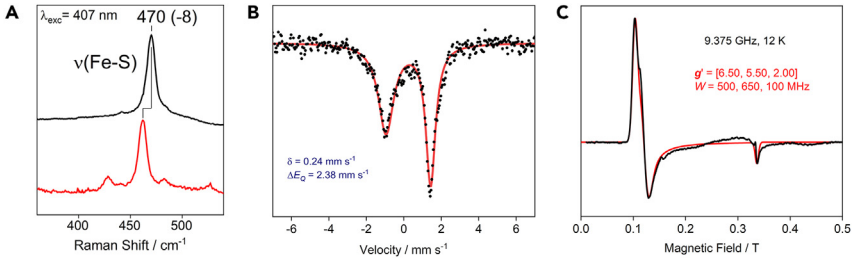

Figure 2. Spectroscopic characterization of sulfido complex 2

(A) Room temperature resonance Raman spectra in THF (black, natural abundance S; red trace is ^{34}S-enriched.

(B) Zero-field ^{57}Fe Mössbauer spectrum at 80 K (black dots; red trace is simulation).

(C) X-band EPR spectrum in frozen toluene/THF (1:1 v/v) solution at 12 K (black; red trace is simulation). Spectral features not reproduced by the simulation correspond to contributions from the disulfide complex **3** as a minor contaminant (Figure S17).

(Table S4). To a first approximation, the electronic structure for the sextet state corresponds to an $(d_{xy}, d_{x^2-y^2})^2(d_{z^2})^1(d_{xz}, d_{yz})^2$ configuration (z axis coincident with the 3-fold symmetry axis, see Figures S27 and S28). Because only three electrons are housed in Fe–S antibonding orbitals, this suggests the presence of a iron-sulfur multiple bond character.

More detailed insight into the electronic structure comes from multireference complete active space self-consistent field (CASSCF) calculations. An active space containing the iron 3d-orbitals and sulfur 3p-orbitals (11 electrons, 8 orbitals) provides ^{57}Fe Mössbauer spectroscopic parameters (δ = 0.23 mm/s; ΔE_Q = −2.28 mm/s) that are in excellent agreement with those observed experimentally (Table S5). Subsequent complete active space self-consistent field/*n*-electron valence state perturbation theory (CASSCF/NEVPT2) calculations indicate that the sextet state is 14.1 kcal/mol more stable than the quartet, and 27.0 kcal/mol more stable than the doublet (Table S6). The dominant configuration (86 %) of the ground sextet state provides further evidence for Fe–S multiple bond character (Figures 3 and S29). The calculations reveal a filled Fe–S σ-bonding molecular orbital that is formed from the iron $3d_{z^2}$ and sulfur $3p_z$ orbitals. The corresponding σ* orbital has admixed iron $4p_z$ orbital character, polarizing it toward the iron atom and reducing its antibonding character. The π bonding manifold is composed of two doubly occupied orbitals that are largely the perpendicular π-bonding combinations of Fe $3d_{xz}/3d_{yz}$ and S $3p_x/3p_y$. The corresponding π* orbitals are each singly occupied. Finally, two electrons are housed in orbitals that are largely the non-bonding combinations of Fe $3d_{xy}/3d_{x^2-y^2}$ and S $3p_x/3p_y$ orbitals.[46] It is worth noting that the sulfur atom character of the singly occupied orbitals results in the transfer of spin density to the sulfido ligand.

This Fe–S multiple bond character is also supported by the results of a natural bond orbital (NBO) analysis, which provides an Fe–S bond order of 2 (Wiberg bond index 1.35) resulting from one filled σ orbital and two half-filled (β-spin) π-symmetry orbitals (Table S7). The computations further indicate that the Fe–S bond is polarized toward the sulfur atom with most of the spin density located on iron (Löwdin spin density 3.883) but with a non-negligible amount on the sulfur ligand (Löwdin spin density 0.696), see Figure S30.

To the best of our knowledge, **2** is the first example of an isolable terminal iron sulfido complex that does not require stabilization from second coordination sphere hydrogen bonding interactions. In contrast to the isoelectronic iron(III) oxo

Please cite this article in press as: Valdez-Moreira et al., Hydrogen atom abstraction by a high-spin [Fe^{III}=S] complex, Chem (2023), https://doi.org/10.1016/j.chempr.2023.05.007

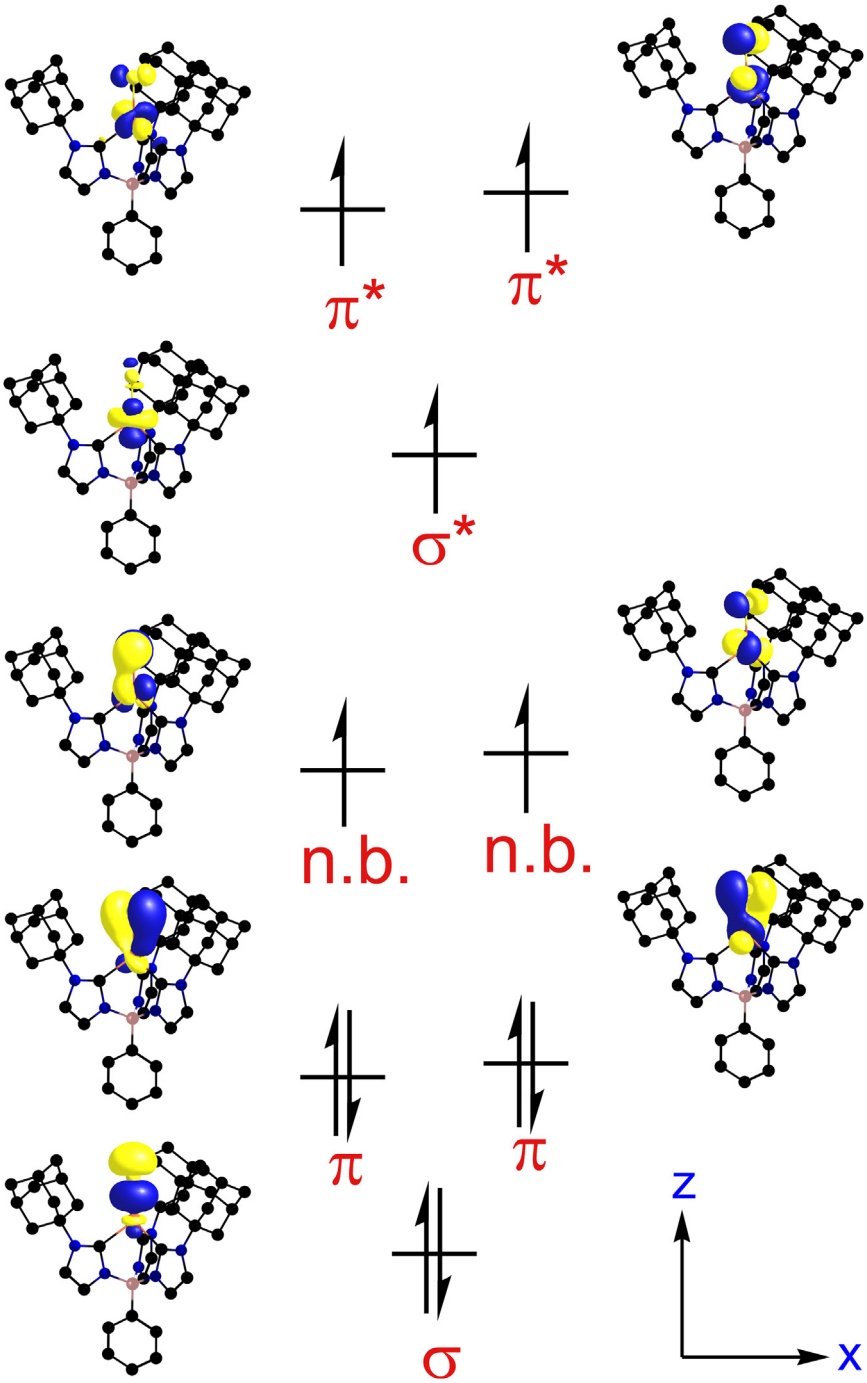

Figure 3. Dominant electronic configuration for 2 (*S* = 5/2), as determined by CASSCF(11,8) calculations, with Fe–S orbital interactions

Hydrogen atoms omitted for clarity. Isodensity 0.05.

complex, which has a low-spin (*S* = 1/2) ground state,[37] complex **2** is high spin (*S* = 5/2), which we attribute to the weaker ligand field strength of the sulfido ligand. Despite the high-spin state, the trigonal pyramidal geometry leads to an electronic structure that allows for Fe–S multiple bond character comprising one σ-bond and two half π-bonds.

Please cite this article in press as: Valdez-Moreira et al., Hydrogen atom abstraction by a high-spin [Fe^{III}=S] complex, Chem (2023), https://doi.org/10.1016/j.chempr.2023.05.007

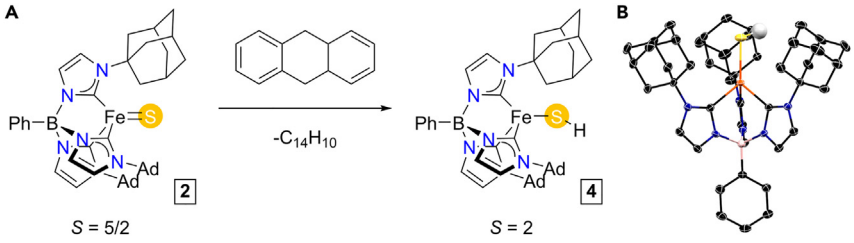

Figure 4. Hydrogen atom abstraction by 2

(A) Reaction of **2** with dihydroanthracene affords the corresponding iron(II) hydrosulfido complex, **4**.

(B) Molecular structure determined by single-crystal X-ray diffraction. Thermal ellipsoids shown at 50% probability, all hydrogen atoms apart from that on the hydrosulfido ligand omitted for clarity.

Complex **2** reacts with an additional 1/8 equiv S_8 to afford the dark brown, intermediate spin (S = 3/2) iron(III) disulfide complex PhB(AdIm)$_3$Fe(κ^2–S_2) (**3**). This complex can also be prepared by reaction of **1** with 1/4 equiv S_8 (Figures S3 and S9). Due to the propensity of sulfur toward catenation (e.g., formation of S_n^{2-} species) small amounts (<5%) of **3** are formed in the synthesis of **2** from **1**. However, in the other direction, complex **3** reacts with **1** to provide the sulfido complex **2** (Figure S2). Complex **3** has been structurally characterized by single-crystal X-ray diffraction (Figure S32; Table S9). The S–S bond distance (2.0339(6) Å) is consistent with the disulfide (S_2^{2-}) oxidation state, which is supported by resonance Raman spectroscopy (ν_{SS} = 541 cm^{-1}, $\Delta^{34}S$ = −16 cm^{-1}) (Figures S12 and S13). This S–S distance is slightly shorter than that for recently reported [Fe(S_2)(CN)$_2$(CO)$_2$]$^{2-}$, likely due to interactions with the counterion in the solid state for the latter, dianionic complex.[47] The frozen toluene EPR spectrum (9.4 GHz, 12 K) of **3** confirms the S = 3/2 state (μ_{eff} = 3.7 μ_B at 298 K), with observed g' = [5.87, 2.05, 1.52] (Figure S17). In contrast to **2**, complex **3** has maximally rhombic symmetry, i.e., $|E/D|$ = 1/3, and D (and E by convention) < 0 (with g_x = 2.050, g_y = 2.078, g_z = 2.149), also with a magnitude of zero-field splitting larger than the microwave quantum energy. An asymmetric doublet is observed in the solid-state ^{57}Fe Mössbauer spectrum at 80 K (Figure S16), with isomer shift (δ = 0.42 mm/s) similar to other five coordinate, S = 3/2 Fe(III) complexes.

The electronic structure of **2**, which localizes spin density to the sulfido ligand, suggests that the complex may be reactive toward hydrogen atom transfer. Indeed, complex **2** reacts with 1/2 equiv 9,10-dihydroanthracene (DHA) to afford the corresponding high-spin (S = 2) iron(II) hydrosulfido complex, PhB(AdIm)$_3$Fe–SH (**4**), see Figures 4 and S10. The structure of **4**, which has been determined by single-crystal X-ray diffraction (Figure S33; Table S10), reveals the same coordination environment around iron as for complex **2**, but with a considerably longer Fe–S distance (2.309(2) Å). This distance is comparable to that reported for the structurally related tris(pyrazolyl)borate complex, Tp^{tBu,Me}FeSH.[48] The hydrosulfido proton was located in the Fourier difference map and was refined freely. The presence of the –SH group is also supported by the Fe–S bond distance of 2.309(1) Å. However, we have been unable to assign ν_{S-H} in the IR spectrum. The Fe–C distances (2.081(4)–2.130(5) Å) in **4** are similar to those in **2**, whereas the B–Fe–S angle is also linear (178.64(9) Å). The complex has also been spectroscopically characterized by ^{1}H NMR spectroscopy and solution magnetometry as a high-spin (S = 2) iron(II) complex (Figures S4 and S5). By contrast, the disulfido complex **3** does not react with DHA.

Three isosbestic points are observed when the reaction between **2** and excess DHA is monitored by UV-vis spectroscopy (Figure S20). The pseudo-first order rate constants

Please cite this article in press as: Valdez-Moreira et al., Hydrogen atom abstraction by a high-spin [Fe^{III}=S] complex, Chem (2023), https://doi.org/10.1016/j.chempr.2023.05.007

are proportional to [DHA], leading to the rate law, rate = $2k_2$[**2**][DHA], with k_2 = 2.3(7) × 10^{-3} $M^{-1}s^{-1}$ at 303 K (Figures S21–S25; Table S1). The rate of reaction with 9,9′,10,10′-tetradeuteroanthracene provides a kinetic isotope effect, k_H/k_D = 2.1 (Figure S26), consistent with rate determining C–H bond cleavage. Although additional investigations are in progress, initial computational investigations point to the viability of a mechanism involving proton-coupled electron transfer. Specifically, gas phase density functional theory (DFT) computations (B3LYP/def2-TZVP) provide an estimate of the S–H bond dissociation free energy for **4** (BDFE = 70 kcal/mol), which is similar to the revised C–H BDFE for dihydroanthracene (72.9 kcal/mol).[49] It is notable that no reaction is observed with toluene or ethylbenzene, in contrast to the iron(III) oxo analog, which forms a stronger O–H bond (BDFE = 82 kcal/mol).[37] Interestingly, the S–H bond in **4** is only slightly weaker than those in organic hydrosulfides (75–85 kcal/mol), in contrast to the O–H bonds of iron hydroxide complexes, which are often significantly weaker than in alcohols.[49] To our knowledge, the only other known values for S–H BDFE in iron complexes are for [2Fe-2S] clusters, specifically $Fe_2(\mu\text{-}SH)_2(CO)_6$ and $Fe_2(\mu\text{-}S)(\mu\text{-}SH)(CO)_6$, which are calculated by DFT to be 72 and 45 kcal/mol, respectively.[47]

Preliminary investigations suggest **2** is a poor sulfur atom transfer reagent. Considering phosphines as classic S-atom acceptors, there is no reaction with bulkier phosphines such as PPh_2Me, likely due to steric reasons. Although minute quantities of $S{=}PMe_3$ (<1 % yield) are observed in the reaction with PMe_3, a number of paramagnetic products are formed, including **4** (Figures S6 and S7).

Conclusions

Structural, spectroscopic, and computational results show that a very bulky tris(carbene)borate ligand stabilizes a terminal iron(III) sulfido complex without the need for second coordination sphere hydrogen bond donors, in contrast to the only previously reported example. Despite a high-spin (S = 5/2) ground state, the strongly axial 3-fold symmetric environment enables Fe=S multiple bond character through one σ- and two half π-bonds, as supported by electronic structure calculations. Initial reactivity studies suggest the accessibility of proton-coupled electron transfer reactions. This reveals the inherent reactivity of the [Fe=S] unit, wherein the multiple bond does not significantly decrease the driving force for S–H bond formation.

EXPERIMENTAL PROCEDURES

Resource availability

Lead contact

Further information and requests for resources should be directed to and will be fulfilled by the lead contact, Jeremy M. Smith (smith962@indiana.edu).

Materials availability

All reagents in this study are either commercially available or can be easily prepared as indicated in the supplemental information.

Data and code availability

Crystallographic data for complexes **2**–**4** have been deposited at the Cambridge Crystallographic Data Center. The CCDC deposition numbers are 2238441–2238443.

SUPPLEMENTAL INFORMATION

Supplemental information can be found online at https://doi.org/10.1016/j.chempr.2023.05.007.

Please cite this article in press as: Valdez-Moreira et al., Hydrogen atom abstraction by a high-spin [Fe^{III}=S] complex, Chem (2023), https://doi.org/10.1016/j.chempr.2023.05.007

ACKNOWLEDGMENTS

Funding from the NSF is gratefully acknowledged by J.A.V.-M., D.C.W., and J.M.S. (CHE-1900020) and by J.T. (grant MCB-1908587). Support for the acquisition of the Bruker Venture D8 diffractometer through the Major Scientific Research Equipment Fund from the President of Indiana University and the Office of the Vice President for Research is gratefully acknowledged. NSF's ChemMatCARS Sector 15 is supported by the NSF Divisions of Chemistry (CHE) and Materials Research (DMR), under grant number CHE-1834750. Use of the Advanced Photon Source, an Office of Science User Facility operated for the DOE Office of Science by Argonne National Laboratory, was supported by DOE under contract no. DE-AC02-06CH11357. We thank Prof. Brian M. Hoffman (Northwestern University, Evanston, IL) for use of EPR/ENDOR spectrometers, which are supported by the the NIH (grant GM-111097).

AUTHOR CONTRIBUTIONS

J.A.V.-M. and D.C.W. designed and performed the synthetic and kinetics experiments, interpreted the results, and assisted with the manuscript. J.M.S. designed and performed the computational investigations and interpreted the results. J.T. collected and interpreted the EPR data. M.P. and V.C. collected and refined the X-ray data. P.M.-L. collected and interpreted the resonance Raman data. J.M.S., P.M.-L. and J.T. wrote the manuscript.

DECLARATION OF INTERESTS

The authors declare no competing interests.

Received: February 8, 2023
Revised: April 25, 2023
Accepted: May 4, 2023
Published: May 31, 2023

REFERENCES

1. Beinert, H., Holm, R.H., and Münck, E. (1997). Iron-sulfur clusters: nature's modular, multipurpose structures. Science *277*, 653–659.
2. Bill, E. (2012). Iron-sulfur clusters—new features in enzymes and synthetic models. Hyperfine Interact. *205*, 139–147. https://doi.org/10.1007/s10751-011-0411-8.
3. Boncella, A.E., Sabo, E.T., Santore, R.M., Carter, J., Whalen, J., Hudspeth, J.D., and Morrison, C.N. (2022). The expanding utility of iron-sulfur clusters: their functional roles in biology, synthetic small molecules, maquettes and artificial proteins, biomimetic materials, and therapeutic strategies. Coord. Chem. Rev. *453*, 214229. https://doi.org/10.1016/j.ccr.2021.214229.
4. Einsle, O., and Rees, D.C. (2020). Structural enzymology of nitrogenase enzymes. Chem. Rev. *120*, 4969–5004. https://doi.org/10.1021/acs.chemrev.0c00067.
5. Van Stappen, C., Decamps, L., Cutsail, G.E., 3rd, Bjornsson, R., Henthorn, J.T., Birrell, J.A., and DeBeer, S. (2020). The spectroscopy of nitrogenases. Chem. Rev. *120*, 5005–5081. https://doi.org/10.1021/acs.chemrev.9b00650.
6. Venkateswara Rao, P.V., and Holm, R.H. (2004). Synthetic analogues of the active sites of iron–sulfur proteins. Chem. Rev. *104*, 527–559.
7. Lee, S.C., Lo, W., and Holm, R.H. (2014). Developments in the biomimetic chemistry of cubane-type and higher nuclearity iron-sulfur clusters. Chem. Rev. *114*, 3579–3600. https://doi.org/10.1021/cr4004067.
8. Vela, J., Stoian, S., Flaschenriem, C.J., Münck, E., and Holland, P.L. (2004). A sulfido-bridged diiron(II) compound and its reactions with nitrogenase-relevant substrates. J. Am. Chem. Soc. *126*, 4522–4523.
9. Rodriguez, M.M., Stubbert, B.D., Scarborough, C.C., Brennessel, W.W., Bill, E., and Holland, P.L. (2012). Isolation and characterization of stable iron(I) sulfide complexes. Angew. Chem. Int. Ed. Engl. *51*, 8247–8250. https://doi.org/10.1002/anie.201202211.
10. Stubbert, B.D., Vela, J., Brennessel, W.W., and Holland, P.L. (2013). A sulfide-bridged diiron(II) complex with a cis-N2H4 ligand. Z. Anorg. Allg. Chem. *639*, 1351–1355. https://doi.org/10.1002/zaac.201300163.
11. Anderson, J.S., and Peters, J.C. (2014). Low-spin pseudotetrahedral iron(I) sites in $Fe_2(\mu$-S) complexes. Angew. Chem. Int. Ed. Engl. *53*, 5978–5981. https://doi.org/10.1002/anie.201401018.
12. Arnet, N.A., Dugan, T.R., Menges, F.S., Mercado, B.Q., Brennessel, W.W., Bill, E., Johnson, M.A., and Holland, P.L. (2015). Synthesis, characterization, and nitrogenase-relevant reactions of an iron sulfide complex with a bridging hydride. J. Am. Chem. Soc. *137*, 13220–13223. https://doi.org/10.1021/jacs.5b06841.
13. DeRosha, D.E., Arnet, N.A., Mercado, B.Q., and Holland, P.L. (2019). A [2Fe-1S] complex that affords access to bimetallic and higher-nuclearity iron-sulfur clusters. Inorg. Chem. *58*, 8829–8834. https://doi.org/10.1021/acs.inorgchem.9b01212.
14. Schneider, C., Demeshko, S., Meyer, F., and Werncke, C.G. (2021). A molecular low-coordinate [Fe-S-Fe] unit in three oxidation states. Chemistry *27*, 6348–6353. https://doi.org/10.1002/chem.202100336.
15. Tang, H., Li, Z., Yang, Y.H., Zhao, Y., Wan, S.Q., Liu, H.L., and Huang, X.R. (2012). Comparison of the FeO(2+) and FeS(2+) complexes in the cyanide and isocyanide ligand environment for methane hydroxylation. J. Comput. Chem. *33*, 1448–1457. https://doi.org/10.1002/jcc.22978.
16. Tang, H., Guan, J., Liu, H., and Huang, X. (2013). Comparative insight into electronic properties and reactivities toward C-H bond activation by iron(IV)-nitrido, iron(IV)-oxo, and iron(IV)-sulfido complexes: a theoretical investigation.

Inorg. Chem. *52*, 2684–2696. https://doi.org/10.1021/ic302766f.

17. Larsen, P.L., Gupta, R., Powell, D.R., and Borovik, A.S. (2004). Chalcogens as terminal ligands to iron: synthesis and structure of complexes with Fe^{III}-S and Fe^{III}-Se motifs. J. Am. Chem. Soc. *126*, 6522–6523.

18. Dey, A., Hocking, R.K., Larsen, P., Borovik, A.S., Hodgson, K.O., Hedman, B., and Solomon, E.I. (2006). X-ray absorption spectroscopy and density functional theory studies of [(H_3buea)Fe^{III}-X]$^{n-}$ (X). J. Am. Chem. Soc. *128*, 9825–9833.

19. Baeza Cinco, M.Á., and Hayton, T.W. (2020). Progress toward the isolation of late metal terminal sulfides. Eur. J. Inorg. Chem. *2020*, 3613–3626. https://doi.org/10.1002/ejic.202000600.

20. Kitajima, N., Fujisawa, K., Tanaka, M., and Morooka, Y. (1992). X-ray structure of thiolatocopper(II) complexes bearing close spectroscopic similarities to blue copper proteins. J. Am. Chem. Soc. *114*, 9232–9233.

21. Fujisawa, K., Moro-Oka, Y., and Kitajima, N. (1994). Formation of a m-h^2:h^2-disulfide dinuclear copper(ii) complex by thermal decomposition of a thiolate complex via C-S bond cleavage. J. Chem. Soc. Chem. Commun. 623–624.

22. Vicic, D.A., and Jones, W.D. (1999). Evidence for the existence of a late-metal terminal sulfido complex. J. Am. Chem. Soc. *121*, 4070–4071.

23. Drobnik, S., Stoll, C., Nöth, H., Polborn, K., Hiller, W., and Lorenz, I.-P. (2006). Photolytisch induzierte Reaktionen von $CpCo(CO)_2$ (Cp = C_5H_5,C_5H_4Me, C_5Me_5 und C5Ph5) mit thiiran zu dinuklearen 1,2-ethandithiolato-S-S-komplexen. Z. Naturforsch. *61b*, 1365–1376.

24. Cho, J., Van Heuvelen, K.M.V., Yap, G.P.A., Brunold, T.C., and Riordan, C.G. (2008). New synthetic routes to a Disulfidodinickel(II) complex: characterization and reactivity of a $Ni_2(\mu$-η^2:η^2-$S_2)$ core. Inorg. Chem. *47*, 3931–3933.

25. Yao, S., Milsmann, C., Bill, E., Wieghardt, K., and Driess, M. (2008). From a paramagnetic, mononuclear supersulfidonickel(II) complex to a diamagnetic dimer with a four-sulfur two-electron bond. J. Am. Chem. Soc. *130*, 13536–13537.

26. Shanahan, J.P., Vicic, D.A., Brennessel, W.W., and Jones, W.D. (2022). Trapping of a late-metal terminal sulfido intermediate with phenyl isothiocyanate. Organometallics *41*, 3448–3453. https://doi.org/10.1021/acs.organomet.2c00435.

27. Hartmann, N.J., Wu, G., and Hayton, T.W. (2015). Synthesis of a "masked" terminal nickel(II) sulfide by reductive deprotection and its reaction with nitrous oxide. Angew. Chem. Int. Ed. Engl. *54*, 14956–14959. https://doi.org/10.1002/anie.201508232.

28. Hartmann, N.J., Wu, G., and Hayton, T.W. (2016). Reactivity of a nickel sulfide with carbon monoxide and nitric oxide. J. Am. Chem. Soc. *138*, 12352–12355. https://doi.org/10.1021/jacs.6b08084.

29. Hartmann, N.J., Wu, G., and Hayton, T.W. (2017). Trapping of an Ni^{II} sulfide by a Co^{I} fulvene complex. Organometallics *36*, 1765–1769. https://doi.org/10.1021/acs.organomet.7b00123.

30. Scepaniak, J.J., Fulton, M.D., Bontchev, R.P., Duesler, E.N., Kirk, M.L., and Smith, J.M. (2008). Structural and spectroscopic characterization of an electrophilic iron nitrido complex. J. Am. Chem. Soc. *130*, 10515–10517.

31. Scepaniak, J.J., Young, J.A., Bontchev, R.P., and Smith, J.M. (2009). Formation of ammonia from an iron nitrido complex. Angew. Chem. Int. Ed. Engl. *48*, 3158–3160.

32. Scepaniak, J.J., Vogel, C.S., Khusniyarov, M.M., Heinemann, F.W., Meyer, K., and Smith, J.M. (2011). Synthesis, structure, and reactivity of an iron(V) nitride. Science *331*, 1049–1052. https://doi.org/10.1126/science.1198315.

33. Smith, J.M., and Subedi, D. (2012). The structure and reactivity of iron nitride complexes. Dalton Trans. *41*, 1423–1429. https://doi.org/10.1039/c1dt11674f.

34. Muñoz, S.B., 3rd, Lee, W.T., Dickie, D.A., Scepaniak, J.J., Subedi, D., Pink, M., Johnson, M.D., and Smith, J.M. (2015). Styrene aziridination by iron(IV) nitrides. Angew. Chem. Int. Ed. Engl. *54*, 10600–10603. https://doi.org/10.1002/anie.201503773.

35. Martinez, J.L., Lin, H.J., Lee, W.T., Pink, M., Chen, C.H., Gao, X., Dickie, D.A., and Smith, J.M. (2017). Cyanide ligand assembly by carbon atom transfer to an iron nitride. J. Am. Chem. Soc. *139*, 14037–14040. https://doi.org/10.1021/jacs.7b08704.

36. Martinez, J.L., Lutz, S.A., Beagan, D.M., Gao, X., Pink, M., Chen, C.H., Carta, V., Moënne-Loccoz, P., and Smith, J.M. (2020). Stabilization of the dinitrogen analogue, phosphorus nitride. ACS Cent. Sci. *6*, 1572–1577.

37. Valdez-Moreira, J.A., Beagan, D.M., Yang, H., Telser, J., Hoffman, B.M., Pink, M., Carta, V., and Smith, J.M. (2021). Hydrocarbon oxidation by an exposed, multiply bonded iron(III) oxo complex. ACS Cent. Sci. *7*, 1751–1755.

38. MacBeth, C.E., Golombek, A.P., Jr., Young, V.G., Yang, C., Kuczera, K., Hendrich, M.P., and Borovik, A.S. (2000). O_2 activation by nonheme iron complexes: a monomeric Fe(III)–oxo complex derived from O_2. Science *289*, 938–941.

39. Matson, E.M., Park, Y.J., and Fout, A.R. (2014). Facile nitrite reduction in a non-heme iron system: formation of an iron(III)-oxo. J. Am. Chem. Soc. *136*, 17398–17401. https://doi.org/10.1021/ja510615p.

40. Gordon, Z., Miller, T.J., Leahy, C.A., Matson, E.M., Burgess, M., Drummond, M.J., Popescu, C.V., Smith, C.M., Lord, R.L., Rodríguez-López, J., et al. (2019). Characterization of terminal iron(III)-oxo and iron(III)-hydroxo complexes derived from O_2 activation. Inorg. Chem. *58*, 15801–15811. https://doi.org/10.1021/acs.inorgchem.9b02079.

41. Reed, C.J., and Agapie, T. (2019). A terminal Fe(III)-oxo in a tetranuclear cluster: effects of distal metal centers on structure and reactivity. J. Am. Chem. Soc. *141*, 9479–9484. https://doi.org/10.1021/jacs.9b03157.

42. Fan, Y., Cheng, J., Gao, Y., Shi, M., and Deng, L. (2018). Iron dinitrogen complexes supported by tris(NHC)borate ligand: synthesis, characterization, and reactivity study. Acta Chim. Sinica *76*. https://doi.org/10.6023/A18030095.

43. Spaeth, A.D., Gagnon, N.L., Dhar, D., Yee, G.M., and Tolman, W.B. (2017). Determination of the Cu(III)-OH bond distance by resonance Raman spectroscopy using a normalized version of Badger's rule. J. Am. Chem. Soc. *139*, 4477–4485. https://doi.org/10.1021/jacs.7b00210.

44. Telser, J. (2017). EPR interactions – zero-field splittings. eMagRes*6*, pp. 207–233.

45. Telser, J. (2018). EPR interactions – zero-field splittings. In EPR Spectroscopy: Fundamentals and Methods, D. Goldfarb and S. Stoll, eds. (John Wiley & Sons, Ltd.), pp. 29–63.

46. Note that symmetry-allowed mixing introduces some sufur p-orbital character to the "non-bonding" orbitals. For more details, see McGarvey, B.R., and Telser, J. (2012). Simple ligand-field theory of d4 and d6 transition metal complexes with a C3 symmetry axis. Inorg. Chem. 51, 6000–6010. 10.1021/ic201189a.

47. Zhang, Y., Woods, T., and Rauchfuss, T.B. (2022). Synthesis and dynamics of ferrous polychalcogenides $[Fe(E_x)(CN)_2(CO)_2]^{2-}$ (E = S, Se, or Te). Inorg. Chem. *61*, 8241–8249. https://doi.org/10.1021/acs.inorgchem.2c00684.

48. Jové, F.A., Pariya, C., Scoblete, M., Yap, G.P., and Theopold, K.H. (2011). A family of four-coordinate iron(II) complexes bearing the sterically hindered tris(pyrazolyl)borato ligand $Tp^{tBu,Me}$. Chemistry *17*, 1310–1318. https://doi.org/10.1002/chem.201001792.

49. Agarwal, R.G., Coste, S.C., Groff, B.D., Heuer, A.M., Noh, H., Parada, G.A., Wise, C.F., Nichols, E.M., Warren, J.J., and Mayer, J.M. (2022). Free energies of proton-coupled electron transfer reagents and their applications. Chem. Rev. *122*, 1–49. https://doi.org/10.1021/acs.chemrev.1c00521.